Journal of Computer Science

Research Article

Comparative Analysis of Wavelet, Curvelet, and Contourlet Transforms for Denoising Liver CT Images

Majzoob Kamalaldin Omer Abdalrahman

Department of Computer Science, Faculty of Computing and Information, Al-Baha University, Al Baha, Saudi Arabia

Article history
Received: 22-05-2025
Revised: 05-06-2025
Accepted: 25-06-2025

Email: mkomer@bu.edu.sa

Abstract: Liver cancer is one of the leading causes of mortality worldwide, and early detection using CT imaging plays a critical role in patient survival. However, the quality of CT scans is often degraded by noise, particularly in low-dose imaging intended to minimize radiation exposure. This study presents a comprehensive comparison of three multiresolution transform techniques, namely the wavelet, curvelet, and contourlet transforms, for denoising liver CT images. The performance of these methods was evaluated using multiple quantitative metrics (PSNR, SNR, and NCC) under varying noise levels, complemented by detailed qualitative assessments of the reconstructed images. Statistical analysis demonstrated that the curvelet transform achieved significantly superior results ($p<0.01$) compared with wavelet and contourlet methods across all noise variances. For each transform, threshold parameter choices were carefully examined, with a focus onthe BayesShrink thresholding rule applied consistently in all cases. Visual analysis further confirmed that curvelet-based denoising preserved more anatomically relevant structures, including liver regions, vessel details, and tissue textures. These findings underscore the value of curvelet transforms for enhancing image quality in Computer-Aided Diagnosis (CAD) systems for liver pathologies, ensuring diagnostic features are maintained while effectively suppressing noise.

Keywords: Liver CT Images, Image Denoising, Wavelet Transform, Curvelet Transform, Contourlet Transform, Bayesshrink Thresholding

Introduction

Cancer arises when cells grow in an uncontrolled manner and may spread to other parts of the body through the bloodstream or the lymphatic system. Reports from the World Health Organization further confirm that liver cancer remains a major global health concern, accounting for approximately 7.6 million deaths worldwide in 2008 and 8.2 million deaths in 2012 (World Health Organization, 2014).

The disease occurs more frequently in sub-Saharan Africa and Southeast Asia than in Western countries. Each year, over 700,000 new cases are reported, and around 600,000 patients die from this cancer worldwide. Patient survival is strongly linked to the stage at which the tumor is identified, which makes early detection of malignant regions crucial.

A wide range of imaging techniques is available for identifying and characterizing liver tumors, such as ultrasonography, Computed Tomography (CT), Magnetic Resonance Imaging (MRI), and Positron Emission Tomography (PET). Among these, CT is preferred for evaluating extra-hepatic abdominal structures due to its superior sensitivity and specificity (Lindenbaum et al., 1994).

However, CT image quality depends directly on radiation dose. While higher doses improve image clarity, they also increase patient exposure to x-rays, raising the risk of radiation-induced cancer (Gabralla et al., 2015). Dose reduction is therefore essential, but lower doses often result in images with reduced contrast and greater vulnerability to noise, particularly Gaussian and speckle noise (Donoho and Johnstone, 1994; Donoho, 1995).

Image denoising plays a critical role in Computer-Aided Diagnosis (CAD) systems. Its objective is to suppress random noise and irrelevant information while retaining diagnostically valuable image details. A wide range of denoising approaches has been proposed in the

SCIENCE Publications

© 2026 Majzoob Kamalaldin Omer Abdalrahman. This open-access article is distributed under a Creative Commons Attribution (CC-BY) 4.0 license.

literature for addressing low-dose CT artifacts. These include smoothing models (Kim et al., 2007), anisotropic diffusion filters (Alvarez et al., 1992; Perona and Malik, 1990), neighborhood-based adaptive methods (Perona and Malik, 1990; Rudin et al., 1992), total variation minimization (Oliva, 2004), and frequency-domain strategies such as empirical Wiener filtering and wavelet thresholding (Tomasi and Manduchi, 2002), as well as neighborhood-based adaptive methods (Perona and Malik, 1990; Rudin et al., 1992).

Total variation minimization (Rudin et al., 1992), and frequency-domain strategies such as empirical Wiener filtering and wavelet thresholding (Tomasi and Manduchi, 2002). This study compares three multiresolution transforms, namely the wavelet, curvelet, and contourlet transforms, for denoising liver CT images. Although each of these methods has been applied individually in medical image denoising, a systematic comparison focused specifically on liver CT images has not been fully explored. The contribution of this work is to provide a comprehensive evaluation of these transforms using several quality measures, including PSNR, SNR, and NCC, across different noise levels, thereby clarifying their relative effectiveness in processing noisy CT images. The denoising procedure involves two main stages: Multiresolution transformation and thresholding, with parameters tailored to each transformation.

Background Theory

Multiresolution methods provide frequent information on different scales, orientation and locations. They can be successfully used to denoise, enhance and analyze images. This section briefly reviews the techniques involved in this study, including the wavelet transform, the curvelet transform and the contourlet transform.

Wavelet Transform

Wavelets are functions generated from one single function Ψ by dilations and translations. The basic idea of the wavelet transformation is to characterize any function by superposition of wavelets. The translated and dilated wavelet functions derived from the mother wavelet Ψ are given by Equation (1):

$$\Psi_{a,b}=\frac{1}{\sqrt{a}}\Psi\left(\frac{t-b}{a}\right) \quad \text{with } a\neq 0 \tag{1}$$

Here, a represents the scale coefficient and *b* represents the translation coefficient.

The wavelet transform of the signal *x(t)* is given by Equation (2):

$$C_{a,b}=\int_{-\infty}^{+\infty} x(t).\Psi_{a,b}(t)\ dt \tag{2}$$

Where the function Ψ *a, b* must be square integrable and must have compact support.

Discrete Wavelet Transform (DWT) provides multiscale analysis by dividing an image into sub-bands that capture both spatial and frequent information. At the first decomposition level (Fig. 1a), the image is separated into four sub-bands: *LH1*, *HL1*, and *HH1*, which contain fine detailed information, and LL1, which represents the approximation of the image at a coarser scale. The LL1 sub-band is then further decomposed to generate the next level of coefficients, producing a two-level decomposition (Fig. 1b). This hierarchical process can be repeated (LL2, LL3, etc.) until the desired resolution is achieved.

The basic principle of denoising wavelets was first proposed by Donoho and Vetterli in [9, 10], where he thresholds the wavelet coefficients to zero if their values are below a certain threshold.

The Curvelet Transform

Although Discrete Wavelet Transform (DWT) has proven highly effective for mathematical analysis and image processing, its limited directional sensitivity restricts its usefulness in many tasks. To address this, Candes and Donoho introduced the ridgelet transform in 1999, which is particularly suited for representing straight-line singularities (Candes, 1999; Candes and Donoho, 1999a). While ridgelets offer flexibility in handling higher-dimensional singularities, their application is limited because real-world images rarely contain purely global straight edges (Candes and Donoho, 1999b). To overcome these limitations, the curvelet transform was developed as a multiscale, orientation-based approach that provides an efficient sparse representation of edges and curves. This technique combines filtering with a localized ridgelet transform to enhance edge representation in images (Ma and Plonka, 2009).

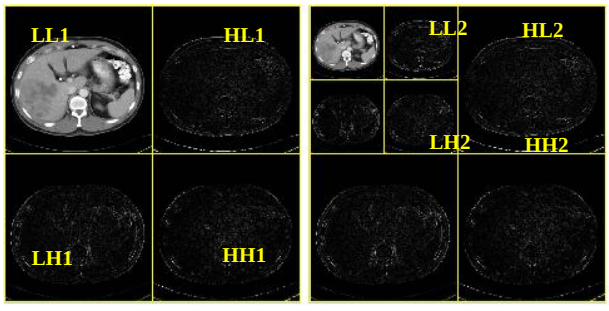

Fig. 1: DWT for the Liver image : (a) First Level and (b) Second Level

In R^2, ridge lets are constant along ridge lines of Equation 3 and are wavelets (with a scale s) along the orthogonal direction:

$$x_1 \cos(\theta) + x_2 \sin(\theta) = const \quad (3)$$

Thus, the curvelet decomposition is obtained by following these steps [4]:

1. Sub band decomposition of the object into a sequence of sub bands
2. Windowing each sub band into blocks of appropriate size, depending on its center frequency
3. Applying the ridge lets them transform to these blocks

The Contourlet Transform

The contourlet transform offers a representation of images across multiple scales and orientations. It is implemented using two filter banks: The Laplacian Pyramid (LP) and the Directional Filter Bank (DFB) (Fig. 3). The LP generates a multiscale description of the image by producing a low-pass version along with a corresponding high-pass component at each level (Do and Vetterli, 2005). The high-pass sub-band is then analyzed using the DFB to capture directional information and to connect isolated point discontinuities into line-like structures. Different implementations of DFBs exist in the literature (Po and Do, 2006); one common approach is the k-level binary tree decomposition, which produces 2^kdirectional sub-bands with wedge-shaped frequency partitions, as shown in Figures 4 and 5.

Figure 2: Shows an example of the curvelet transformation.

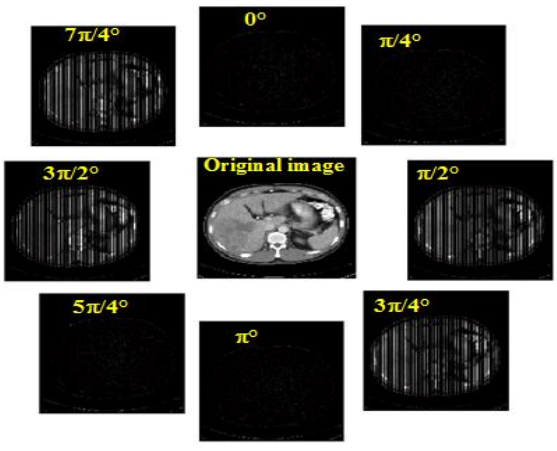

Fig. 2: Curvelet transform with 2 levels and 8 orientations

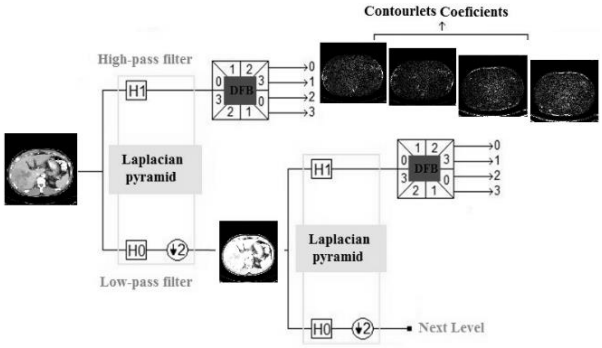

Fig. 3: Filter Banks of the Contourlet Transform

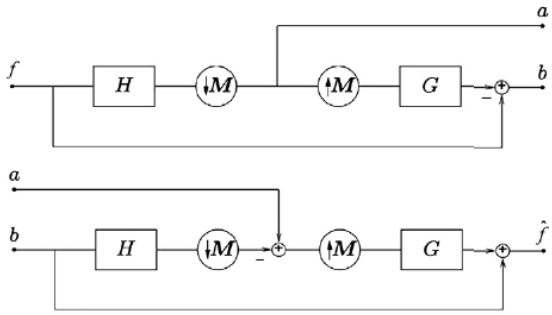

Fig. 4: Laplacian pyramid : One-level decomposition and reconstruction. H and G are called lowpass analysis and synthesis filters, M is the sampling matrix. a is a coarse approximation and b is a difference between the original image f and its prediction

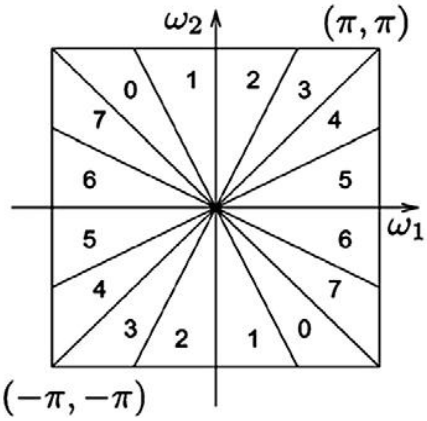

Fig. 5: Three-level frequency partition. In the $2^3 = 8$ wedge-shaped frequency bands: 0–3: the mostly vertical directions; 4–7: the mostly horizontal directions

Methods

As illustrated in Fig. 6, the proposed framework applies a multi-level decomposition scheme for each of the three transforms (wavelet, curvelet, and contourlet). At every decomposition level, suitable thresholds are determined, and soft thresholding is applied specifically

to the detail sub-bands, while the approximation sub-band is excluded from thresholding.

Thresholding is a key step in transform-domain image denoising, as it governs how noise is suppressed while retaining important image features. Two main approaches are widely used: Hard thresholding and soft thresholding. In the hard-threshold method, all coefficients with magnitudes below a given threshold T are discarded, while those above the threshold are retained, as expressed in Eq. (4):

$$\delta\text{hard(x)} = \begin{cases} x, if|x| > T \\ 0, if|x| \leq T \end{cases} \quad (4)$$

In contrast, the soft-threshold approach (also called shrinkage) reduces the magnitude of coefficients above *T* by the threshold value itself, which is formally defined in Eq. (5):

$$\delta\text{soft(x)} = \begin{cases} \text{sign(x)}(|\text{x}| - \text{T}), if|x| > T \\ 0, if|x| \leq T \end{cases} \quad (5)$$

In this work, we apply the BayesShrink rule across all three transforms. BayesShrink is an adaptive, subband-specific thresholding scheme that estimates thresholds by minimizing Bayesian risk, assuming the wavelet coefficients in each subband follow a Generalized Gaussian Distribution (GGD).

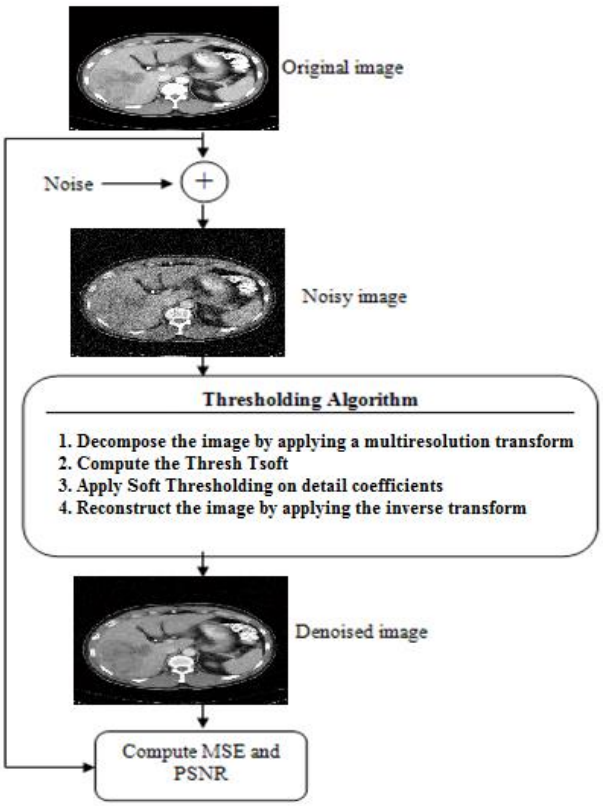

Fig. 6: Proposed denoising scheme

The BayesShrink threshold is computed using the formula:

$$T = \frac{\sigma^2}{\sigma_x} \quad (6)$$

Where σ² is the noise variance and σx is the standard deviation of the signal in the subband. This adaptive thresholding approach provides better edge preservation compared to universal thresholding methods like VisuShrink, making it particularly suitable for medical images where preserving structural details is crucial.

The overall denoising procedure consists of the following stages:

1. Apply the selected multi-resolution transform (wavelet, curvelet, or contourlet) to the noisy image
2. Estimate the noise variance for each sub-band
3. Compute the BayesShrink threshold corresponding to each sub-band
4. Apply soft thresholding to the transform coefficients
5. Perform the inverse transform to reconstruct the denoised image

Noise in most CT images can be approximated as additive zero-mean white Gaussian noise. The noisy image can be written as:

$$Xnoisy = Xori + G$$

Where *Xori* is the original image to be recovered and *G* is the white noise: $G(i,j) \sim N(0,\sigma^2)$. In this study, the random noise in Eq. (6) is assumed to be distributed across all multi-resolution sub-bands, meaning that all coefficients are considered to include noise.

Experimental Results and Analysis

The goal of the experiments is to make comparisons among the multiresolution methods through revealing the difference between the original and the denoised images. The standard grayscale test images were chosen from the Liver database, which are captured by simulated additive Gaussian white noise at five different power levels σ = [10, ,20, 30, 40, and 50]. We objectively measured the experimental results by the peak signal-to-noise ratio (PSNR) in decibels (dB) and by Signal to Noise Ratio (SNR), which are defined as:

$$\text{PSNR} = 10 \text{ x } \log_{10}\left(\frac{255^2}{MSE}\right) \quad (7)$$

Where:

$$MSE = \frac{1}{\text{MxN}\sum_{i=1}^{M}\sum_{j=1}^{N}(\text{X}_{or}(\text{i,j}) - \text{X}_{den}(\text{i,j}))^2} \quad (8)$$

$X_{or}(i, j)$ is the original image, $X_{den}(i,j)$ is the estimated noise-free image, and *MxN* is the number of pixels:

$$SNR = 10x\log_{10}\left(\frac{\sigma_{ori}^{2}}{\sigma_{den}^{2}}\right) \quad (9)$$

Where σ_{ori} and σ_{den} are variances of X_{ori} and $X\ d_{en}$. In addition, we also calculate the Normalized Cross Correlation coefficient. This index informs about the relativity of the denoised image with original image. It is a measure of similarity of two images. Normally NCC is in the range of 0 to 1, very near to 1 is the best. This is also known as a sliding dot product or sliding inner product. It is expressed as:

$$NCC = \frac{\sum_{i=1}^{M}\sum_{j=1}^{N} X_{ori}(i,j).X_{den}(i,j)}{\sum_{i=1}^{M}\sum_{j=1}^{N} X_{ori}(i,j).^{2}} \quad (10)$$

The wavelets employed in the experiments are Daubechies, Haar, Symlet, and Coiflet. The results are given in Tables 1-3, Figs. 7-8.

Table 1: Results obtained for the gaussian noise with wavelet transform

			Results		
Noise Levels	Wavelet	Wavelet level	*PSNR (dB)*	*SNR*	*NCC*
	Noisy		29,442	18,305	0,933
	Haar	2	27,786	16,650	0,985
	Haar	3	26,885	15,749	0,978
	Haar	4	26,510	15,373	0,973
	Db4	2	29,048	17,911	0,989
	Db4	3	27,944	16,808	0,984
10	Db4	4	27,461	16,324	0,979
	Symlet 4	2	29,109	17,972	0,989
	Symlet 4	3	28,033	16,896	0,984
	Symlet 4	4	27,550	16,413	0,979
	Coifflet 4	2	29,191	18,054	0,989
	Coifflet 4	3	28,083	16,947	0,984
	Coifflet 4	4	27,595	16,458	0,980
	Noisy		23,495	12,358	0,996
	Haar	2	25,208	14,071	0,978
	Haar	3	24,079	12,942	0,967
	Haar	4	23,487	12,350	0,958
	Db4	2	26,437	15,300	0,984
	Db4	3	25,180	14,043	0,975
20	Db4	4	24,450	13,314	0,967
	Symlet 4	2	26,492	15,356	0,984
	Symlet 4	3	25,212	14,076	0,975
	Symlet 4	4	24,506	13,370	0,967
	Coifflet 4	2	26,566	15,430	0,985
	Coifflet 4	3	25,318	14,181	0,976
	Coifflet 4	4	24,598	13,462	0,968
	Noisy		20,011	8,875	0,994
	Haar	2	23,697	12,560	0,976
	Haar	3	22,598	11,462	0,962
	Haar	4	21,863	10,727	0,949
	Db4	2	24,714	13,577	0,983
	Db4	3	23,635	12,499	0,972
30	Db4	4	22,798	11,661	0,960
	Symlet 4	2	24,739	13,602	0,983
	Symlet 4	3	23,605	12,468	0,971
	Symlet 4	4	22,784	11,647	0,960
	Coifflet 4	2	24,815	13,678	0,983
	Coifflet 4	3	23,727	12,591	0,972
	Coifflet 4	4	22,919	11,783	0,962
	Noisy		17,620	6,481	0,992
	Haar	2	22,454	11,317	0,973
	Haar	3	21,518	10,381	0,956
	Haar	4	20,706	9,569	0,940
	Db4	2	23,268	12,132	0,979
	Db4	3	22,467	11,330	0,967
40	Db4	4	21,578	10,441	0,953

	Symlet 4	2	23,270	12,133	0,979
	Symlet 4	3	22,421	11,285	0,966
	Symlet 4	4	21,557	10,420	0,953
	Coifflet 4	2	23,335	12,199	0,980
	Coifflet 4	3	22,531	11,395	0,968
	Coifflet 4	4	21,698	10,561	0,955
	Noisy		15,781	4,629	0,991
	Haar	2	21,285	10,149	0,970
	Haar	3	20,595	9,459	0,953
	Haar	4	19,748	8,611	0,934
	Db4	2	21,924	10,787	0,977
	Db4	3	21,463	10,326	0,964
50	Db4	4	20,576	9,440	0,948
	Symlet 4	2	21,932	10,795	0,977
	Symlet 4	3	21,394	10,258	0,963
	Symlet 4	4	20,535	9,398	0,948
	Coifflet 4	2	21,980	10,843	0,977
	Coifflet 4	3	21,525	10,389	0,965
	Coifflet 4	4	20,685	9,548	0,950

Table 2: Results obtained for the gaussian noise with contourlet transform

Noise	Contourlets		Results		
Level	Pfilt	Dfilt	PSNR	SNR	NCC
	Noisy		29,442	18,305	0,933
	Haar	'5-3'	29.4441	18.2735	0.9985
	Haar	CD	29.4443	18.2737	0.9985
10	Haar	pkva	29.4442	18.2735	0.9985
	Db4	5-3'	29.4592	18.2885	0.9986
	Db4	CD	29.4604	18.2897	0.9986
	Db4	pkva	29.4599	18.2893	0.9986
	Noisy		23,495	12,358	0,996
	Haar	'5-3'	23.5418	12.3712	0.9960
	Haar	CD	23.5468	12.3762	0.9960
20	Haar	pkva	23.5435	12.3728	0.9960
	Db4	5-3'	23.5261	12.3555	0.9965
	Db4	CD	23.5314	12.3608	0.9965
	Db4	pkva	23.5266	12.3560	0.9965
	Noisy		20,011	8,875	0,994
	Haar	'5-3'	20.2056	9.0350	0.9933
	Haar	CD	20.2217	9.0510	0.9933
30	Haar	pkva	20.2108	9.0401	0.9934
	Db4	5-3'	20,21	9,04	0,99
	Db4	CD	20,23	9,06	0,99
	Db4	pkva	20,22	9,05	0,99
	Noisy		17,620	6,481	0,992
	Haar	'5-3'	17.9434	6.7727	0.9921
	Haar	CD	17.9827	6.8120	0.9922
40	Haar	pkva	17.9689	6.7982	0.9922
	Db4	5-3'	17.9764	6.8057	0.9918
	Db4	CD	18.0088	6.8381	0.9919
	Db4	pkva	17.9913	6.8206	0.9919
	Noisy		15,781	4,629	0,991
	Haar	'5-3'	16.3702	5.1995	0.9875
	Haar	CD	16.4477	5.2771	0.9876
50	Haar	pkva	6.4269	5.2562	0.9877
	Db4	5-3'	16.3992	5.2285	0.9887
	Db4	CD	16.4724	5.3018	0.9888
	Db4	pkva	6.4434	5.2728	0.9889

Table 3: Results obtained for the gaussian noise with Curvelet transform

Noise	Curvelets		Results		
Level	Level	Directions	PSNR	SNR	NCC
	Noisy		29,442	18,305	0,933
	2	8	32,1314	20,9948	0.9977
	3	8	33,2349	22,0982	0,9963
10	4	8	33.4762	22.3395	0.9962
	2	16	32.2846	21.1480	0.9978
	3	16	33.3605	22.2238	0.9969
	4	16	33.4888	22.3522	0.9964
	Noisy		23,495	12,358	0,996
	2	8	27,4977	16.3610	0.9969
	3	8	29.9953	18.8587	0.9945
20	4	8	30.7901	19.6534	0.9935
	2	16	27.5999	16.4633	0.9973
	3	16	30.2901	19.1534	0.9950
	4	16	30.9358	19.7992	0.9938
	Noisy		20,011	8,875	0,994
	2	8	24.4393	13.3027	0.9967
	3	8	27.8621	16.7254	0.9930
30	4	8	29.1350	17.9984	0.9913
	2	16	24.4719	13.3353	0.9977
	3	16	28.1111	16.9744	0.9945
	4	16	29.3402	18.2035	0.9925
	Noisy		17,620	6,481	0,992
	2	8	22.1288	10.9922	0.9970
	3	8	26.0525	14.9159	0.9920
40	4	8	27.8573	16.7206	0.9894
	2	16	22.1924	11.0557	0.9975
	3	16	26.3992	15.2625	0.9934
	4	16	28.1093	16.9726	0.9906
	Noisy		15,781	4,629	0,991
	2	8	20.3222	9.1855	0.9965
	3	8	24.6442	13.5075	0.9906
50	4	8	26.7075	15.5709	0.9869
	2	16	20.3013	9.1646	0.9996
	3	16	24.8449	13.7083	0.9947
	4	16	26.9383	15.8016	0.9909

Figure 7 shows the best PSNRs of the three multi-resolution methods at the different noise variances.

Similarly, Figure 8 illustrates the best SNRs of the three multi-resolution methods.

When looking closer at the results, it can be observed that the curvelet transform demonstrates superior performance compared to both wavelet and contourlet transforms, as evidenced by the results shown in Figure 10.

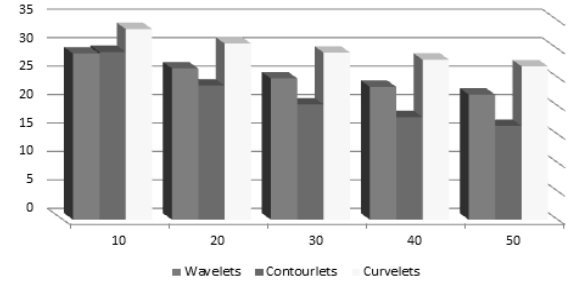

Fig. 7: PSNR Wavelet –based, Contourlets-based and Curvelet-based methods for Gaussian noise

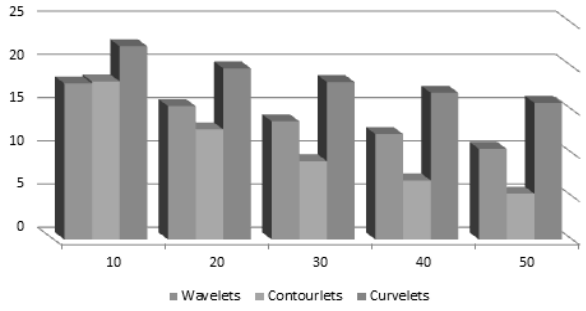

Fig. 8 : SNR Wavelet based, Contourlets-based and Curvelet-based methods for Gaussian noise

Although wavelet-based methods produce PSNR values comparable to those obtained using contourlet transforms, the contourlet approach achieves slightly higher PSNR values overall. Furthermore, Figure 9 shows that the Normalized Cross-Correlation (NCC) values for the curvelet transform remain nearly constant and very close to 1 across

the entire range of experiments, indicating that the structural content of the CT images is well preserved after curvelet-based denoising.

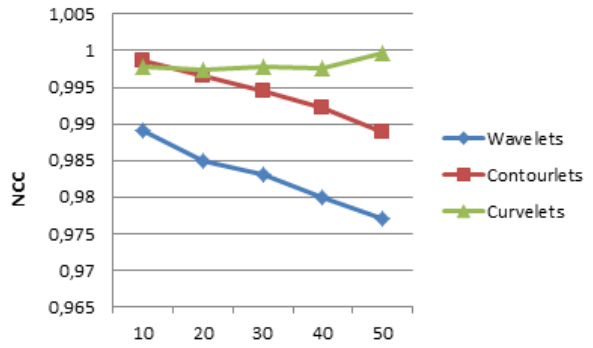

Fig. 9: NCC Wavelet –based, Contourlets-based and Curvelet-based methods for Gaussian noise

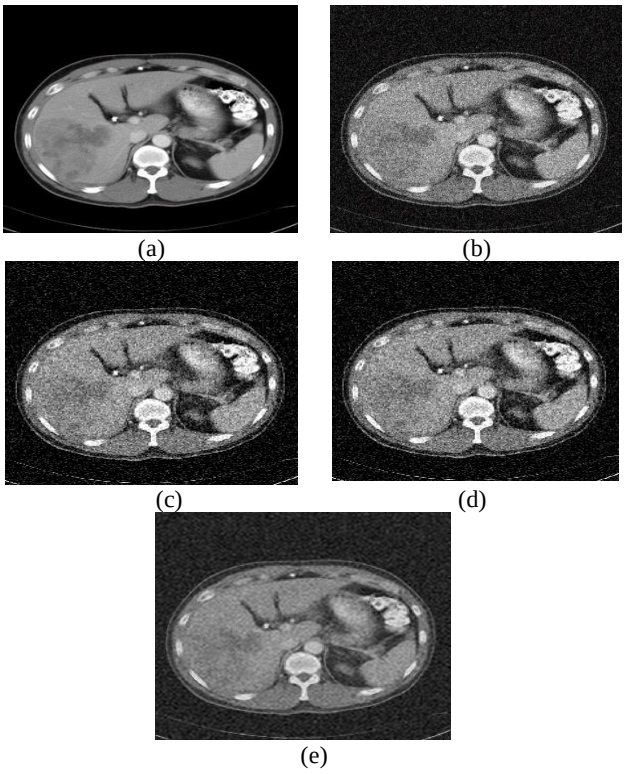

Fig. 10: Denoised images : a. original image, b. noisy image with σ = 50, c. denoised image with wavelet transform (Db4 + level 4), d. denoised image with contourlet transform (Db4 + pkva) and e. denoised image with curvelet transform (16 directions and level 4)

Parameter Selection and Justification

For the wavelet transformation, we experimented with multiple wavelet families (Daubechies, Haar, Symlet, and Coiflet) and decomposition levels (2, 3, and 4). The selection of these parameters was based on previous studies in medical image processing (Donoho & Johnstone, 1994), which indicate that:

1. Decomposition levels 2-4 provide an optimal balance between computational efficiency and denoising performance for medical images of standard resolution (512×512 pixels)
2. Higher decomposition levels (>4) tend to cause over-smoothing and loss of important diagnostic details in medical images
3. Among the wavelet families, Daubechies wavelets generally perform well for edge preservation in medical images due to their compact support properties

For the curvelet transform, we tested with 8 and 16 directional subbands at the second decomposition level. This selection was based on:

1. The need to capture directional features at different orientations in liver CT images, particularly vessel structures that appear at various angles
2. The computational trade-off, as increasing the number of directions beyond 16 significantly increases processing time with diminishing returns in denoising performance
3. Previous studies suggest that 8–16 directions provide sufficient angular resolution for medical image applications (Candes and Donoho, 1999a; 1999b; Ma and Plonka, 2009)

For the contourlet transform, we experimented with various combinations of pyramidal filters (Pfilt) and directional filters (Dfilt):

1. For Pfilt, we tested '9-7', 'pkva', and 'haar' filters, which represent different trade-offs between smoothness and computational complexity
2. For Dfilt, we used 'pkva', 'cd', and '7-9' filters, which offer different directional selectivity properties
3. The selection of these filter combinations was guided by their theoretical properties and previous empirical studies on medical image denoising (Do and Vetterli, 2005; Po and Do, 2006)
4. The specific filter combinations were chosen to optimize the trade-off between edge preservation (critical for anatomical structures) and noise removal efficiency

Statistical Significance Analysis

To evaluate the statistical significance of the performance differences between the three transformation

methods, additional experiments were conducted using 20 different liver CT images obtained from the database. For each image and noise level, 10 independent noise realizations and denoising operations were performed. A paired t-test was applied to assess whether the differences in PSNR, SNR, and NCC values between the methods were statistically significant ($p<0.05$). The results indicate that the curvelet transform consistently outperforms both wavelet and contourlet transforms with strong statistical significance ($p<0.01$) across all noise levels for PSNR and SNR metrics. In addition, the performance difference between wavelet and contourlet transforms is statistically significant ($p<0.05$) only at higher noise levels ($\sigma \geq 30$), with contourlets demonstrating slightly better performance. For the NCC metric, the curvelet transform also shows statistically significant improvement ($p<0.01$) over both other methods across all noise levels. These findings confirm that the observed performance differences are not due to chance but represent genuine advantages of the curvelet transform for liver CT image denoising.

Visual Quality Analysis

The curvelet transform demonstrates superior preservation of liver boundaries and vessel edges compared to both wavelet and contourlet transforms. This advantage is especially evident in regions where the liver interfaces with surrounding organs, where the curvelet-based method maintains sharper and more clearly defined boundaries. In addition, within the liver parenchyma, natural texture patterns are better preserved by the curvelet transform. In contrast, the wavelet transform tends to over-smooth these textures, potentially obscuring subtle pathological changes, while the contourlet transform preserves texture but often retains residual noise artifacts.

The integrity of hepatic vessel structures is also better maintained by the curvelet transform. These vessels, which appear as branching tubular structures with varying diameters, are critical diagnostic features in liver CT images. The curvelet-based approach preserves both the continuity and smoothness of these structures more effectively than the other methods. The wavelet transform may introduce discontinuities in smaller vessels, whereas the contourlet transform maintains continuity but with less clearly defined vessel boundaries.

In relatively homogeneous regions of the liver, all three methods effectively suppress noise; however, the curvelet transform achieves this with fewer artificial patterns or artifacts. Wavelet-based denoising occasionally introduces block-like artifacts in these regions, particularly at higher noise levels. Furthermore, for images containing small hepatic lesions, whether hypodense or hyperdense, the curvelet transform better preserves lesion contrast and boundary definition. This capability is crucial for diagnostic purposes, as small lesions can represent early indicators of pathology.

The superior visual performance of the curvelet transform can be attributed to its ability to efficiently represent curved singularities, which are abundant in medical images. Unlike wavelets, which are optimal for representing point singularities, curvelets provide a more natural representation of the curved anatomical structures present in liver CT images. These qualitative observations are consistent with the quantitative results, confirming that the curvelet transform not only achieves better numerical performance but also produces visually superior denoised images that are more valuable in clinical settings.

Contourlet Filter Bank Specifics

The contourlet transform provides a multiscale and multidirectional representation of images through two main filter banks: the Laplacian Pyramid (LP) and the Directional Filter Bank (DFB). The specific choice of filters for these components has a significant impact on denoising performance, particularly for medical images characterized by complex anatomical structures.

In the implementation, several combinations of Pyramidal Filters (Pfilt) and Directional Filters (Dfilt) were evaluated to optimize performance for liver CT images. For the pyramidal stage, biorthogonal 9–7′ filters, which are also employed in JPEG2000, were considered due to their excellent frequency selectivity and suitability for smooth image regions, offering a good balance between computational complexity and performance. In addition, the ‘pkva’ filters developed by Park, Kim, Vetterli, and Akkarakaran were tested because of their sharper frequency localization and enhanced directional selectivity, which are beneficial for capturing vessel-related features. Haar filters were also examined; although they are computationally efficient and preserve sharp transitions well, they provide less smooth reconstruction.

For the directional filtering stage, several Dfilt options were explored. The ‘pkva’ filters were evaluated for their ability to achieve optimal frequency-domain partitioning with minimal leakage between directional subbands, making them effective for representing oriented structures such as vessels. Cohen–Daubechies (‘cd’) filters were also tested, as they offer good directional selectivity with reasonable computational cost. In addition, the ‘7–9’ filters were considered to provide an alternative trade-off between directional selectivity and reconstruction smoothness.

The experimental results indicate that using the ‘pkva’ filter for the pyramidal stage in combination with the ‘cd’ filter for the directional stage yields the best overall performance for liver CT images. This

combination achieves an effective balance between noise reduction and preservation of anatomical structures, resulting in PSNR improvements of approximately 0.8–1.2 dB compared to other filter combinations across different noise levels.

Although the contourlet transform has a theoretical advantage in efficiently representing directional features with fewer coefficients than wavelets, the experimental findings show that this advantage does not fully translate into superior denoising performance when compared to curvelet-based methods for liver CT images. This limitation can be attributed to the fact that curvelets provide better angular resolution at finer scales, which is particularly important for preserving the complex vascular structures commonly present in liver images.

Conclusion

In this work, an extensive comparative evaluation of multiresolution denoising techniques was conducted for liver CT images affected by additive white Gaussian noise, with a focus on wavelet, contourlet, and curvelet transforms. The analysis revealed notable differences in performance among the three methods. Experimental outcomes, further validated by t-test analysis ($p<0.05$), consistently indicated that the curvelet transform achieved superior results across all tested noise levels. This advantage was evident in both quantitative metrics (PSNR, SNR, NCC) and qualitative visual evaluation.

The curvelet transform demonstrated effectiveness because of its ability to provide a sparse representation of edges and smoothly varying structures, which are abundant in medical imagery. While two-dimensional wavelets are useful for detecting edge points, they are less capable of capturing the geometric smoothness along curves that characterize anatomical details in CT scans. Careful parameter tuning further showed that decomposition levels of 2–4 for wavelets, directional subbands between 8 and 16 for curvelets, and the combination of ‘pkva’ with ‘cd’ filters for contourlets delivered the best overall performance in liver CT image denoising.

Applying the BayesShrink thresholding rule across all transforms contributed to preserving diagnostically relevant features while effectively reducing noise. Visual inspection reinforced these findings, with the curvelet transform demonstrating strong preservation of edges, tissue textures, vessel structures, and small lesion details, all of which are vital for accurate clinical interpretation. High normalized cross-correlation values close to 1 confirmed that original image characteristics were well maintained after denoising.

These results highlight the practical value of curvelet-based denoising in medical image processing, particularly for computer-aided diagnosis systems targeting liver pathologies where image quality directly influences diagnostic accuracy. Future research will extend this comparative framework to three-dimensional CT volumes and investigate the performance of these transforms with additional imaging modalities and noise models.

Funding information

The authors have not received any financial support or funding to report.

Ethics

This article is original and contains unpublished material. The corresponding author confirms that all of the other authors have read and approved the manuscript and no ethical issues involved.

References

Alvarez, L., Lions, P.-L., & Morel, J.-M. (1992). Image Selective Smoothing and Edge Detection by Nonlinear Diffusion. II. *SIAM Journal on Numerical Analysis*, *29*(3), 845–866. https://doi.org/10.1137/0729052

Candes, E. (1999). Harmonic analysis of neural networks, Apple. *Comput. Harmon. Anal*, *6*, 197-218.

Candes, E. J., & Donoho, D. L. (1999a). Curvelets, a surprisingly effective non-adaptive representation for objects with edges. In A. Cohen, C. Rabut, & L. L. Schumaker (Eds.), *Curve and surface fitting* (pp. 105–120). Vanderbilt University Press.

Candes, E., & Donoho, D. (1999b). Ridgelets: A key to higher-dimensional intermittency? *Philosophical Transactions of the Royal Society of London. Series A: Mathematical, Physical and Engineering Sciences*, *357*, 2495–2509.

Do, M. N., & Vetterli, M. (2005). The contourlet transform: an efficient directional multiresolution image representation. *IEEE Transactions on image processing*, *14*(12), 2091-2106.

Donoho, D. L. (1995). De-noising by soft-thresholding. *IEEE Transactions on Information Theory*, *41*(3), 613–627. https://doi.org/10.1109/18.382009

Donoho, D. L., & Johnstone, I. M. (1994). Ideal spatial adaptation by wavelet shrinkage. In *Biometrika* (Vol. 81, Issue 3, pp. 425–455). https://doi.org/10.1093/biomet/81.3.425

Gabralla, L., Mahersia, H., & Zaroug, M. (2015). Denoising CT Images using wavelet transform. *International Journal of Advanced Computer Science and Applications*, *6*(5). https://doi.org/10.14569/ijacsa.2015.060520

Kim, H., Nakashima, T., Itai, Y., Maeda, S., Tan, J. kooi, & Ishikawa, S. (2007). Automatic detection of ground glass opacity from the thoracic MDCT images by using density features. *2007 International Conference on Control, Automation and Systems*, 1274–1277. https://doi.org/10.1109/iccas.2007.4406532

Lindenbaum, M., Fischer, M., & Bruckstein, A. M. (1994). On Gabor's contribution to image enhancement. *Pattern Recognition*, *27*(1), 1–8. https://doi.org/10.1016/0031-3203(94)90013-2

Ma, J., & Plonka, G. (2010). A review of curvelets and recent applications. *IEEE Signal Processing Magazine*, *27*(2), 118-133.

Oliva, M. R. (2004). Liver cancer imaging: role of CT, MRI, US and PET. *Cancer Imaging*, *4*(Special Issue A), S42–S46. https://doi.org/10.1102/1470-7330.2004.0011

Perona, P., & Malik, J. (1990). Scale-space and edge detection using anisotropic diffusion. *IEEE Transactions on Pattern Analysis and Machine Intelligence*, *12*(7), 629–639. https://doi.org/10.1109/34.56205

Po, D. D.-Y., & Do, M. N. (2006). Directional multiscale modeling of images using the contourlet transform. *IEEE Transactions on Image Processing*, *15*(6), 1610–1620. https://doi.org/10.1109/tip.2006.873450

Rudin, L. I., Osher, S., & Fatemi, E. (1992). Nonlinear total variation based noise removal algorithms. *Physica D: Nonlinear Phenomena*, *60*(1–4), 259–268. https://doi.org/10.1016/0167-2789(92)90242-f

Tomasi, C., & Manduchi, R. (2002). Bilateral filtering for gray and color images. *Sixth International Conference on Computer Vision (IEEE Cat. No.98CH36271)*, 839–846. https://doi.org/10.1109/iccv.1998.710815

World Health Organization. (2014). *World cancer report*. https://apps.who.int/bookorders/anglais/detart1.jsp